TECHNICAL MEMORANDUM

468

A fast radiative transfer model for the assimilation of limb radiances from MIPAS: Accounting for horizontal gradients

Niels Bormann and Sean B. Healy

Research Department

June 2005

European Centre for Medium-Range Weather Forecasts
Europäisches Zentrum für mittelfristige Wettervorhersage
Centre européen pour les prévisions météorologiques à moyen terme

Series: ECMWF Technical Memoranda

A full list of ECMWF Publications can be found on our web site under:
http://www.ecmwf.int/publications/

Contact: library@ecmwf.int

European Centre for Medium-Range Weather Forecasts
Shinfield Park, Reading, RG2 9AX, England

Abstract

We investigate the influence of horizontal structure in the atmosphere on the simulation of emitted infrared limb radiances from the Envisat-MIPAS instrument, and examine a pragmatic extension of the regression-based RTMIPAS fast radiative transfer model to deal with horizontal atmospheric structure. The pragmatic extension of RTMIPAS takes into account the horizontal structure at the ray-tracing step, but uses regression models derived from a set of horizontally homogeneous atmospheres in the transmittance parameterisation. This reduces the computational effort required for the derivation of the regression models. The effects of horizontal gradients in the atmosphere on MIPAS radiances are examined by comparing radiance spectra simulated with RTMIPAS to line-by-line equivalents and to real MIPAS observations.

It is shown that neglecting horizontal structure in the atmosphere can introduce errors in the radiance simulation that exceed by far the instrument noise, particularly for lower tangent heights and for strongly absorbing spectral regions. The pragmatic extension of the fast radiative transfer model can substantially reduce this error, and for tangent pressures less than 350 hPa (tangent heights greater than about 8 km) almost all error due to horizontal gradients is eliminated. In agreement with this, fast-model radiances simulated from cross-sections of the ECMWF model compare significantly better to observed MIPAS limb radiances than radiances simulated under the assumption of horizontal homogeneity. This further confirms a considerable reduction in forward-model error when horizontal atmospheric structure is taken into account.

1 Introduction

Growing interest in monitoring the chemical composition and thermal structure of the stratosphere from space has sparked increased efforts to optimise the use of data from passive limb sounders such as the Michelson Interferometer for Passive Atmospheric Sounding (MIPAS) on Envisat or the Microwave Limb Sounder (MLS) on EOS-Aqua. The attraction of the limb-viewing geometry stems from long ray paths in the tangent layer, which maximises the emitting material that is sensed, so that temperature can be measured at higher altitudes and even minor gases can be detected (e.g., Kidder and Vonder Haar 1995).

Limb observations are inherently sensitive to the vertical as well as the horizontal structure of the atmosphere being sensed. The scale of the influence of the horizontal structure is highly dependent on the characteristics of the spectral regions used, as a simple consideration of typical weighting functions reveals (e.g., Livesey and Read 2000). For channels in spectral regions with relatively weak absorption, the associated weighting functions along the line-of-sight peak around the tangent point. This translates to sharp weighting-function peaks at the tangent height against a vertical coordinate, yet fairly broad weighting in the horizontal, with most information originating from a region of typically 500 km located almost symmetrically around the tangent point (see, for instance, the MIPAS channel at 941.050 cm^{-1}, indicated as dashed line in Fig. 1). In contrast, channels in more strongly absorbing spectral regions show weighting functions that may peak well away from the tangent point, on the side towards the instrument (see, for instance, the MIPAS channel at 704.875 cm^{-1}, indicated as solid line in Fig. 1). In addition, if we consider an entire vertical scan of a limb sounder, each field of view may not have the same sub-tangent point, adding further dependency on spatial atmospheric structures. This feature is usually referred to as tangent-point drift and it depends on the adopted scanning pattern (e.g., Livesey and Read 2000, Carlotti et al. 2001). If the instrument is not viewing within the orbital plane, a vertical scan is even sensitive to the 3-dimensional structure of the atmosphere. Despite all this, many retrieval schemes for rearward or forward viewing limb sounders assume that horizontal gradients in the atmosphere can be neglected for one limb scan (e.g., Ridolfi et al. 2000, von Clarmann 2003), and this leads to a situation-dependent retrieval error.

The role of horizontal gradients in limb sounding has been recognised for some time (e.g., Gill and House 1971, Marks and Rodgers 1993). As a result, methods have been developed which retrieve the horizontal gradient as well as the vertical representation (e.g., Marks and Rodgers 1993). More recently, tomographic

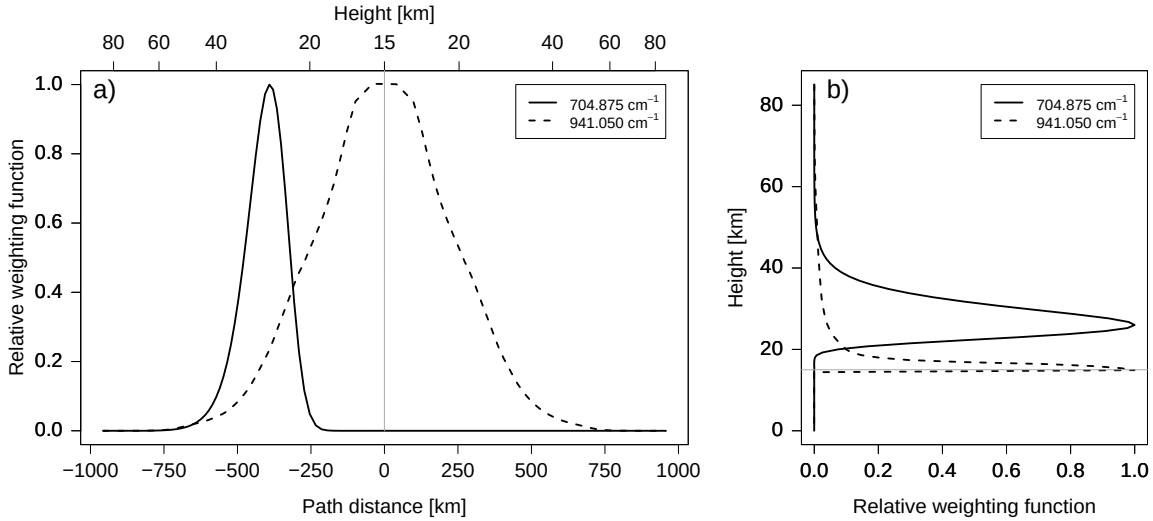

Figure 1: a) Weighting functions for two sample channels from MIPAS at a tangent altitude of 15.0 km as a function of line-of-sight distance. MIPAS is located towards lower values of the line-of-sight distance, and the tangent point is situated at 0.0 km (grey line). The weighting functions have been normalised to 1.0 at the maximum for display purposes. The calculations are based on a midlatitude reference profile, and the two channels are examples for spectral regions with relatively strong (704.875 cm^{-1}) and relatively weak absorption (941.050 cm^{-1}), respectively. b) As a), but as a function of height.

retrieval methods have become feasible. These treat simultaneously a series of adjacent limb scans (or even an entire orbit), and retrieve a representation of the atmosphere on a grid covering the vertical as well as the orbital coordinate (e.g., Livesey and Read 2000, Carlotti et al. 2001, Reburn et al. 2003). The studies show considerable benefits from this approach as a result of eliminating the error arising from neglecting horizontal gradients. Improvements in terms of the horizontal resolution that can be retrieved compared to treating each limb scan individually have also been shown (Ridolfi et al. 2004). For MLS on EOS-Aura, the routine retrieval processing is based on a tomographic approach (Livesey and Wu 1999).

Recently, ECMWF has started developments to directly assimilate infrared limb radiances from MIPAS within a global numerical weather prediction (NWP) model. To achieve this, a new fast radiative transfer model to compute MIPAS limb radiances has been developed and extensively validated (Bormann et al. 2004 and 2005, hereinafter BMH04 and BMH05, respectively). The model is referred to as RTMIPAS, and its development and validation were restricted to atmospheres without horizontal gradients. Forward modelling approaches similar to RTMIPAS have been investigated for MLS on EOS-Aura (Liang Feng 2004, pers. communication). Given that accounting for 2-dimensional (vertical and horizontal) structure of the atmosphere has led to benefits in a retrieval framework, there is some interest to similarly account for horizontal gradients in the future assimilation of limb radiances.

In this report we investigate the role of horizontal structure in the atmosphere on the fast simulation of emitted infrared limb radiances from the MIPAS instrument. We quantify the error made in the radiance simulation by assuming horizontal homogeneity. We also investigate a pragmatic extension of the RTMIPAS model to take into account 2-dimensional atmospheric structure encountered by rearward or forward-looking limb sounders. The approach adopted for the extension avoids the costly retraining of the regressions used in RTMIPAS and thus simplifies the derivation of the transmittance parameterisation. It is the first time that a regression-based radiative transfer model for MIPAS has been extended to take into account 2-dimensional atmospheric structure.

We also present first comparisons between observed MIPAS radiances and radiances simulated with RTMIPAS from ECMWF model fields.

The structure of the report is as follows: We first provide a summary of the RTMIPAS methodology, outline our strategy for the extension to treat horizontal gradients, provide detail about the methods adapted for the ray-tracing, and introduce the LBL calculations performed for this study. Next, we provide an estimate for errors introduced by neglecting horizontal gradients in limb radiative transfer models, and give estimates for the errors introduced through the fast transmittance parameterisation in the 2-dimensional version of RTMIPAS. Comparisons between simulated and observed MIPAS radiances further highlight the benefits of the 2-dimensional version of RTMIPAS. A summary and our conclusions are given in the last section.

2 Methodology

2.1 RTMIPAS

The MIPAS instrument on-board Envisat is an interferometer with very high spectral resolution (0.025 cm^{-1}, unapodised), measuring infrared limb radiances in 5 spectral bands between 685 and 2410 cm^{-1}, giving a total of 59,605 spectral points (i.e., channels). In the normal scanning pattern, MIPAS provides observations at tangent altitudes between 6 an 68 km, with a field of view (FOV) of 3 km in the vertical and 30 km in the horizontal at the tangent point. Further details about the instrument can be found in ESA (2000).

RTMIPAS is a fast radiative transfer model for the simulation of emitted clear-sky apodised limb radiances from MIPAS, and its methodology is discussed in detail in BMH04 and BMH05; here we present only a brief summary of the main points. RTMIPAS follows the methodology of RTTOV (Radiative Transfer for TOVS) which is used for the direct assimilation of nadir radiances at several operational NWP centres (e.g., Saunders et al. 1999, Matricardi et al. 2004). RTMIPAS represents the atmosphere on 81 fixed pressure levels and, for each channel, calculates convolved level-to-satellite transmittances from each level based on linear regression models for the effective layer optical depths in each layer. The regression models are derived from a large database of line-by-line (LBL) model calculations for a set of diverse profiles, with local horizontal homogeneity assumed in the calculations. The predictors used in the regression models represent layer quantities as well as values characterising the conditions along the ray towards the observer. Ray-tracing is required to obtain the ray path and to construct the predictors. Radiative transfer calculations are performed for rays with tangent points at a subset of 34 of the fixed pressure levels, and the resulting radiance/tangent height relationship is subsequently convolved with the MIPAS FOV function to obtain the FOV radiances. Comparisons between radiances simulated with RTMIPAS and radiances calculated from a LBL model show that the error introduced through the fast transmittance parameterisation is well below the noise level of the MIPAS instrument for most channels and tangent heights. In the following, this first version of RTMIPAS will be referred to as 'RTMIPAS-1d' to highlight that local horizontal homogeneity is assumed.

2.2 Approach to extend RTMIPAS to 2-dimensional atmospheres

One way to extend RTMIPAS to the 2-dimensional geometry is to extend the required ray-tracing to the 2-dimensional geometry, and to retrain the regression models based on LBL calculations for a set of diverse atmospheric cross-sections. While this approach is likely to give the smallest fast model errors, it has a considerable disadvantage: LBL calculations for all MIPAS channels for atmospheres with horizontal gradients are very costly. The required computational resources would be significantly higher than the already very large effort invested in the 1-dimensional calculations, both in terms of the size of the transmittance database as well as

the computing time. Also, additional effort would be required to construct a set of atmospheric cross-sections that suitably captures the atmospheric variability, in terms of both the vertical and the horizontal structure.

Instead, we investigate here a more pragmatic and cost-effective extension to the 2-dimensional geometry: we replace only the ray-tracing used in RTMIPAS-1d with a full 2-dimensional ray-tracer, outlined in the next subsection and further in the Appendix, and we use the same regression models with the same coefficients as in RTMIPAS-1d. We will refer to the resulting model as 'RTMIPAS-2d'. The hypothesis behind the approach is that the regression models should be adequate for an atmosphere with horizontal gradients, as long as the atmospheric variability on both sides of the tangent point was captured in the training set used for the RTMIPAS-1d regression models. The 2d-extension adds only marginally to the execution time of RTMIPAS, since all additional computations are confined to the ray-tracing which in typical applications contributes less than 1.5 % of the computation time (depending on the number of channels/tangent heights being modelled).

2.3 Ray-tracing in 2-dimensional atmospheres on a pressure grid

The computation of the path-lengths, Δs, between the fixed pressure levels used in RTMIPAS-1d is outlined in BMH05 (Appendix A). Using plane polar-coordinates (r, θ), it is shown that Δs can be evaluated in terms of the change in ray bending, $\Delta\alpha$, which in turn is related to the radial gradient of refractive-index, n. In the 1-dimensional case, the radial gradients are evaluated from the profile information at the assumed tangent point location. By definition, the angular position within the measurement plane, θ, is not required because refractive index is only a function of radius, $n(r)$. The calculation of path-lengths in RTMIPAS-2d is essentially based on the same approach (see Appendix). However, ray bending at an arbitrary point on the two dimensional ray-path, $P(r, \theta)$, is calculated using refractive index gradients at $P(r, \theta)$, instead of using the values at the ray tangent point. In addition, the impact parameter defined as $a = nr\sin\phi$ (n is the refractive index and ϕ is the angle between the tangent of the ray-path and local radius vector) varies along the ray-path as a result of the horizontal gradients. The variation is given by (e.g., Healy 2001):

$$\frac{da}{ds} = \left(\frac{\partial n}{\partial \theta}\right)_r \tag{1}$$

2.4 Line-by-line calculations for a set of cross-sections

To evaluate the approach used for RTMIPAS-2d we compare RTMIPAS-2d-simulated radiances with results from LBL computations for 40 cross-sections taken from ECMWF 12-h forecast fields. The cross sections provide diverse conditions of temperature, humidity, and ozone, covering the period 1 September 2003 to 1 July 2004, with dates and coordinates of the centres of the cross-sections given in Table 1. Each cross section consists of 41 profiles at 40 km spacing oriented in North-South direction through the central point, to simulate a simplified MIPAS rearward viewing orientation. The first 10 cross-sections have been subjectively sampled to represent situations with considerable horizontal structure, whereas the others have been selected to adequately cover different seasons and geographical regions. Note that most cross-sections sample the period 15 October 2003 - 1 March 2004, during which MIPAS near-realtime ozone retrievals were assimilated operationally at ECMWF in addition to NOAA-16 SBUV profiles (Dethof 2003). The operational ECMWF model at the time had a resolution of T511 (approx. 40 km) in the horizontal, and 60 levels in the vertical, with a top of the model at 0.1 hPa. To extrapolate onto the RTMIPAS pressure levels above the forecast model's top we used a constant mesospheric lapse rate for temperature, and kept humidity and ozone constant.

It is worth noting that while we endeavoured to cover all geographical regions and seasons in the set of 40 cross-sections, no effort has been made to specifically optimise the atmospheric variability represented in this

Table 1: Dates and locations of the centre of the cross sections used for model intercomparison calculations.

No.	Date and time (UTC)	Latitude [°N]	Longitude [°E]	No.	Date and time (UTC)	Latitude [°N]	Longitude [°E]
1	20030901 00	-65.00	140.00	21	20031101 12	70.00	25.00
2	20031001 00	-60.00	10.00	22	20031201 12	-60.00	-160.00
3	20031201 00	50.00	-30.00	23	20031201 12	-20.00	-5.00
4	20031201 00	75.00	-75.00	24	20031201 12	20.00	0.00
5	20040201 00	40.00	-165.00	25	20040101 12	-85.00	-72.00
6	20040201 00	60.00	90.00	26	20040101 12	-55.00	30.00
7	20040501 00	-45.00	-30.00	27	20040101 12	0.00	20.00
8	20040501 00	10.00	-140.00	28	20040101 12	30.00	-50.00
9	20040701 00	-51.00	-122.00	29	20040101 12	55.00	-70.00
10	20040701 00	50.00	-20.00	30	20040101 12	85.00	50.00
11	20031015 12	-75.00	20.00	31	20040201 12	-40.00	50.00
12	20031015 12	-50.00	80.00	32	20040201 12	-30.00	-100.00
13	20031015 12	-10.00	-60.00	33	20040201 12	-20.00	-150.00
14	20031015 12	5.00	-55.00	34	20040301 12	-50.00	-73.00
15	20031015 12	40.00	60.00	35	20040301 12	-15.00	50.00
16	20031015 12	80.00	-120.00	36	20040301 12	-5.00	105.00
17	20031101 12	-75.00	151.00	37	20040301 12	55.00	-125.00
18	20031101 12	-40.00	175.00	38	20040301 12	70.00	130.00
19	20031101 12	10.00	150.00	39	20040401 12	-30.00	130.00
20	20031101 12	30.00	90.00	40	20040401 12	20.00	42.00

diverse set of cross-sections. To do so, methods such as used in Chevallier (2002) could be adopted, but this is beyond the scope of the present study. Visual inspection showed that the set of central profiles exhibits a similar variability as the dataset used for the training of RTMIPAS, and this dataset was sampled using the method of Chevallier (2002).

The LBL calculations for the cross-sections were performed using the Reference Forward Model (RFM[1]; Dudhia et al. 2002b), a multi-purpose LBL radiative transfer model originally based on GENLN2 (Edwards 1992). The configuration used for the RFM is the same as in BMH05, except that now the atmospheric conditions are specified through the 41 profiles describing each cross-section (the satellite is located northward of the central profile), and a Runge-Kutta 4th order numerical integration is adopted to perform the 2-dimensional ray tracing. Note that for the RFM calculations the 41 profiles of the cross-section needed to be interpolated to the height levels of the central profile, whereas the RTMIPAS calculations use the RTMIPAS fixed pressure levels as vertical coordinate. For the fixed gases included in the calculations (i.e. gases other than water vapour and ozone), the same constant and horizontally homogeneous climatology has been used as in BMH05. We perform calculations for rays with infinitesimal small FOVs ("pencil beams") for the same tangent pressures as in BMH05. Tangent point drift is not included in these calculations; instead, all tangent points are located along the central profile. The LBL calculations are performed for all MIPAS channels in the wavenumber range 685-1750 cm^{-1}; channels for the MIPAS D band have been excluded to save computational cost. Channels in the MIPAS D band show poor signal-to-noise characteristics and many are affected by solar effects, and they will therefore not be used in the planned assimilation.

[1] Documentation of the RFM can be found on www.atm.ox.ac.uk/RFM/sum.html.

3 Results

3.1 Influence of horizontal gradients

Before validating RTMIPAS-2d radiances against RFM-2d equivalents, it is worthwhile to compare RTMIPAS-1d radiances for the set of 40 cross-sections with the 2-dimensional RFM calculations, to characterise the error that is introduced through neglecting horizontal gradients. To do this, we performed RTMIPAS-1d calculations for the set of cross-sections, using the central profile to establish a horizontally homogeneous atmosphere. Figures 2 and 3 show the standard deviation of the RTMIPAS-1d minus RFM-2d radiance differences, normalised by the apodised instrument noise (i.e., error-to-noise ratio). For the noise specification, in-flight values of the well-studied orbit 2081 have been used (see Fig. 1 in BMH05). For display purposes, we show the maximum and the mean value for each 40-channel interval (1 cm^{-1}) for each pencil beam. As pointed out in BMH05, displaying the maximum in each 40-channel interval emphasises the largest errors (as just one channel with a large error may represent the whole spectral interval). In the present comparison, the poorest performance is likely to be found for the most strongly absorbing channel, as this will show the strongest errors arising from horizontal gradients, as discussed earlier.

The statistics demonstrate that neglecting horizontal gradients in RTMIPAS can introduce a substantial error, and the error is larger the lower the tangent altitude (Figures 2 and 3). Standard deviations for the RTMIPAS-1d minus RFM-2d radiance difference for the lowest pencil beams exceed the instrument noise for the majority of channels (e.g., Fig. 4), with some channels exhibiting error-to-noise ratios of 10.0 and higher. Such error-to-noise ratios are much larger than the error introduced through the fast transmittance parameterisation in RTMIPAS (cf, Figures 34 and 35 in BMH04). As expected, the error is largest in spectral regions with strong absorption, and higher pencil beams show statistics which are more in-line with values obtained previously in the validation of RTMIPAS-1d for horizontally homogeneous atmospheres (cf, Figures 34 and 35 in BMH04). The size of the error is also considerably dependent on the channel (e.g., Fig. 4), and for pencil beams with tangent pressures of less than 121.10 hPa a sizeable number of channels can be found for which the error-to-noise ratio is below 1.0, most of which are located in the water vapour bands. The RTMIPAS-1d simulations also exhibit a considerable positive bias in the most strongly absorbing spectral regions (Fig. 5).

The error introduced through horizontal gradients is of course dependent on the atmospheric situation, and its size depends on the magnitude and shape of the gradients in the sampled cross-section. Larger errors typically occur in midlatitudes and along the edges of the polar vortices. For cases for which the atmosphere changes non-linearly with the horizontal coordinate even weakly absorbing channels whose weighting functions peak fairly symmetrically around the tangent point may exhibit a larger error. For actual MIPAS observations, the sign of the error also depends on the viewing direction, with descending and ascending nodes of the satellite's orbits typically showing opposite signs for the same geographical region.

3.2 Validation of RTMIPAS-2d against LBL radiances

The RTMIPAS-2d radiances compare substantially better with the 2-dimensional LBL calculations than the RTMIPAS-1d radiances. Figures 6 to 10 show that error-to-noise ratios calculated from RTMIPAS-2d minus RFM-2d radiance differences are much smaller than error-to-noise ratios for RTMIPAS-1d for all pencil beams and all spectral regions (compare Figures 6 and 7 to Figures 2 and 3, respectively). For most channels and pencil beams with tangent pressures above 350 hPa (typically 8.0-8.5 km) RTMIPAS-2d can reproduce the LBL radiance spectra to a level of accuracy that is below the noise level of the MIPAS instrument.

The evaluation of RTMIPAS-2d for the set of cross-sections can be compared to the validation of RTMIPAS-1d

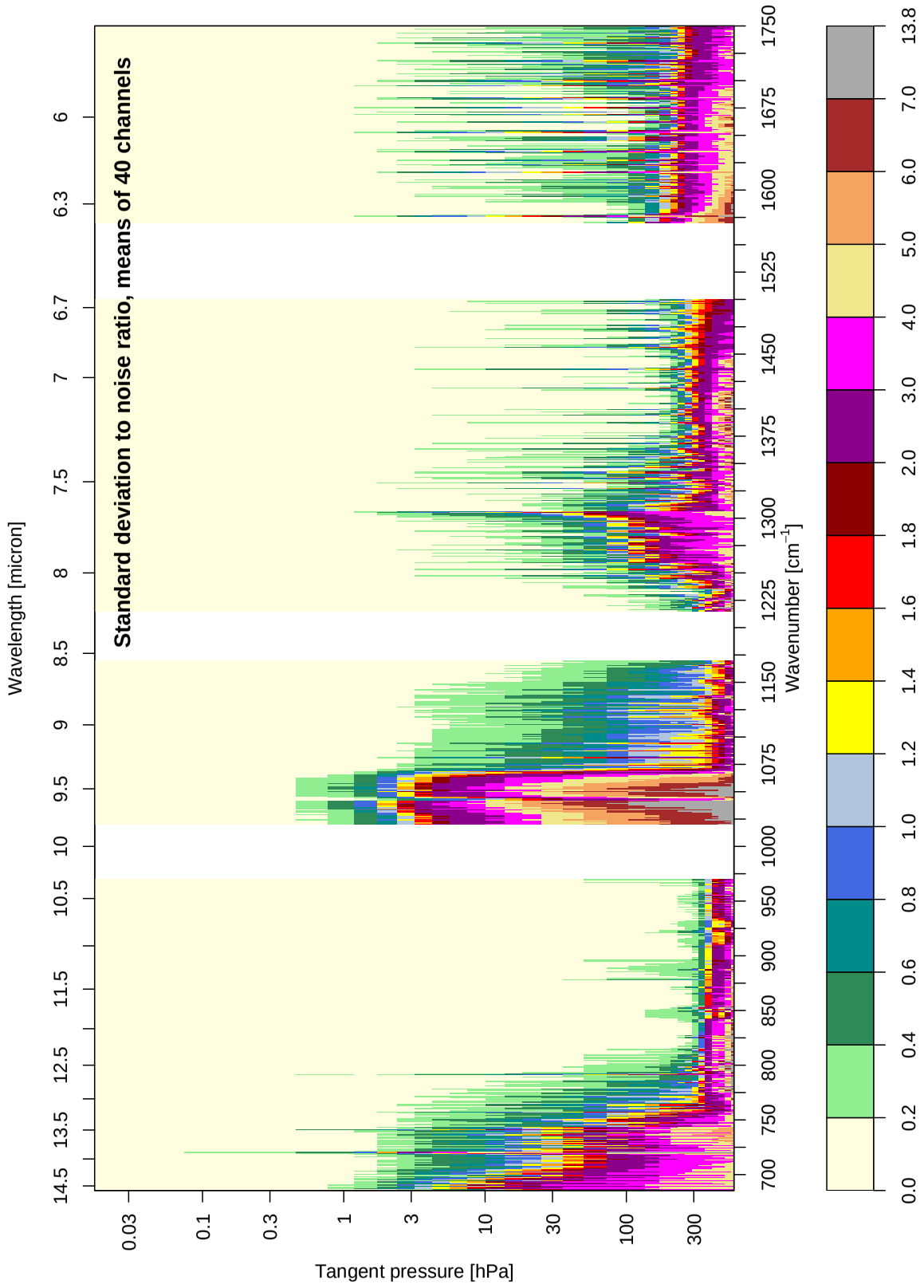

Figure 2: Standard deviation of the RTMIPAS-1d minus RFM-2d radiance differences, scaled by the MIPAS noise, for the set of 40 diverse cross-sections. The plot shows the mean standard deviation to noise ratio over 40 channel intervals (i.e., 1 cm^{-1} intervals) as a function of wavenumber and pencil-beam pressure. Note the non-linear colour scale.

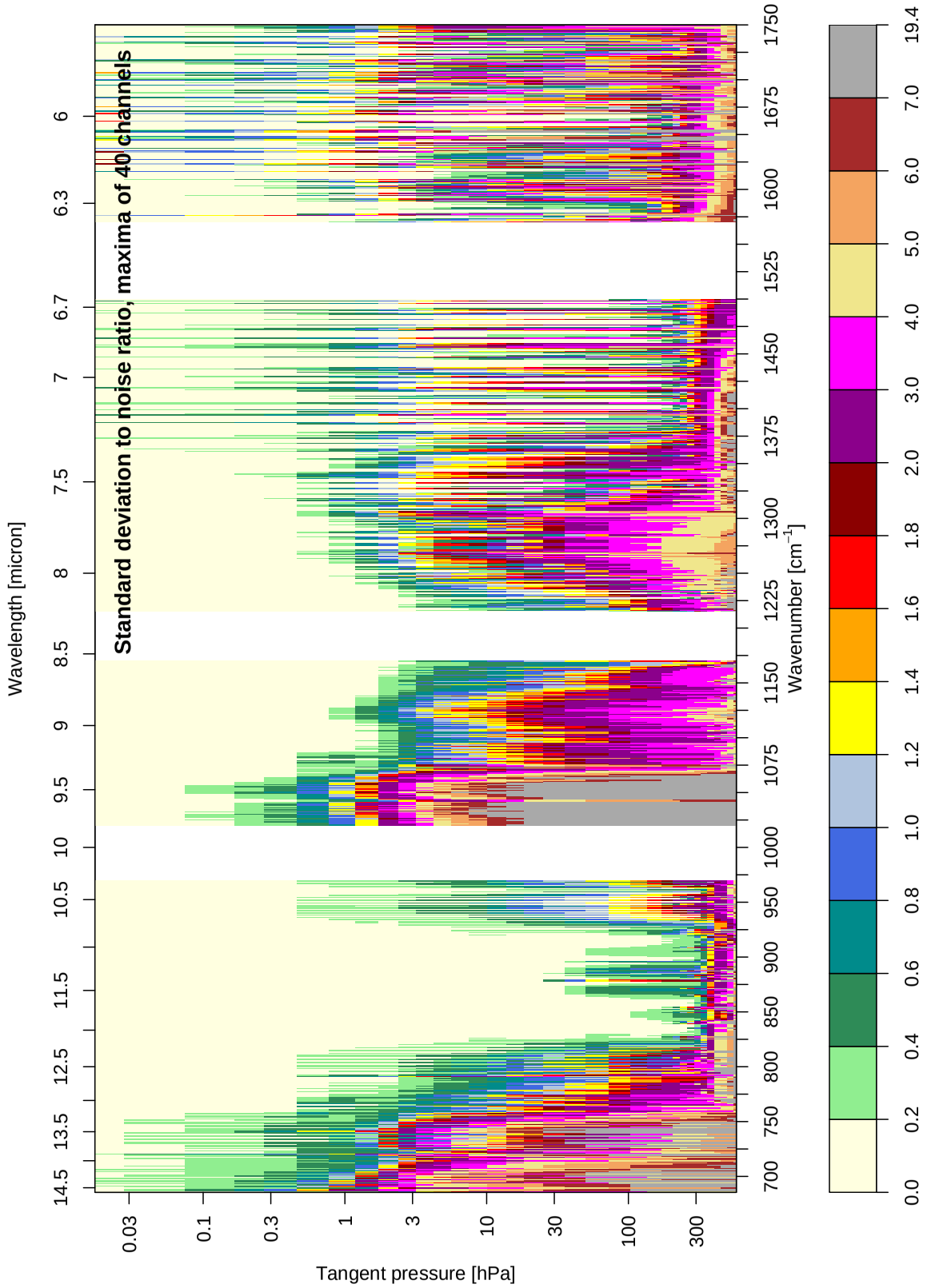

Figure 3: As Fig. 2, but for the maximum standard deviation to noise ratio over 40 channel intervals (i.e., 1 cm^{-1} intervals).

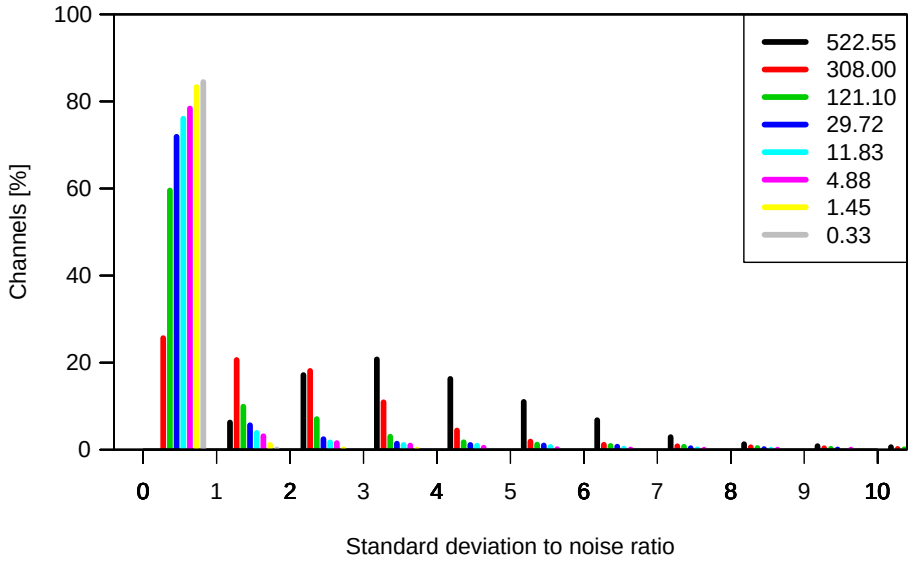

Figure 4: Distribution of the number of channels [%] versus the standard deviation of the RTMIPAS-1d minus RFM-2d radiance differences, scaled by the MIPAS noise. Results for 8 selected pencil beams are shown, with their tangent pressures [hPa] indicated in the legend. The binning interval is 1.0.

against LBL calculations for the horizontally homogeneous case, based on the statistics presented in BMH04 for an independent profile set. A comparison of Figures 6 to 10 with Figures 36 to 40 in BMH04 reveals that RTMIPAS-2d compares similarly well with the 2-dimensional RFM LBL calculations as RTMIPAS-1d did for horizontally homogeneous atmospheres, at least for tangent pressures above 350 hPa. As in RTMIPAS-1d, error-to-noise ratios are largest in the 750-800 cm^{-1} wavenumber region with pencil-beam tangent pressures around the tropopause level. Slightly larger biases than in the 1-dimensional case are observed for some channels in the water vapour bands. For very high pencil beams (tangent pressures above 0.3 hPa), the error to noise ratios for RTMIPAS-2d shows somewhat different behaviour than found in the RTMIPAS-1d evaluation, with significantly lower values in the CO_2 band, and larger values for some channels in the MIPAS C band (1570-1750 cm^{-1}). This is most likely an artefact of the simplistic extrapolation applied in our cross-sections above the ECMWF model top. In contrast, the profiles used in BMH04 were complemented by profiles from the HALogen Occultation Experiment (HALOE) on board the Upper Atmosphere Research Satellite (UARS) and therefore exhibit different variability.

The findings demonstrate that for tangent pressures above 350 hPa our pragmatic approach of extending RTMIPAS to 2-dimensional atmospheres performs well, and RTMIPAS-2d is able to eliminate most error otherwise introduced through the assumption of local horizontal homogeneity (compare, for instance, Figures 3 and 7). The results suggest that for layers above 350 hPa little could be gained by re-deriving the regression models used in RTMIPAS on the basis of 2-dimensional atmospheres.

For the lowest pencil beams with tangent pressures larger than 350 hPa the RTMIPAS-2d radiances compare significantly more poorly with LBL equivalents than was the case for the horizontally homogeneous calculations. The most likely explanation for this is that the sample of cases used to derive the regression models for the lowest RTMIPAS layers does not capture all variability encountered in RTMIPAS-2d, especially in the case

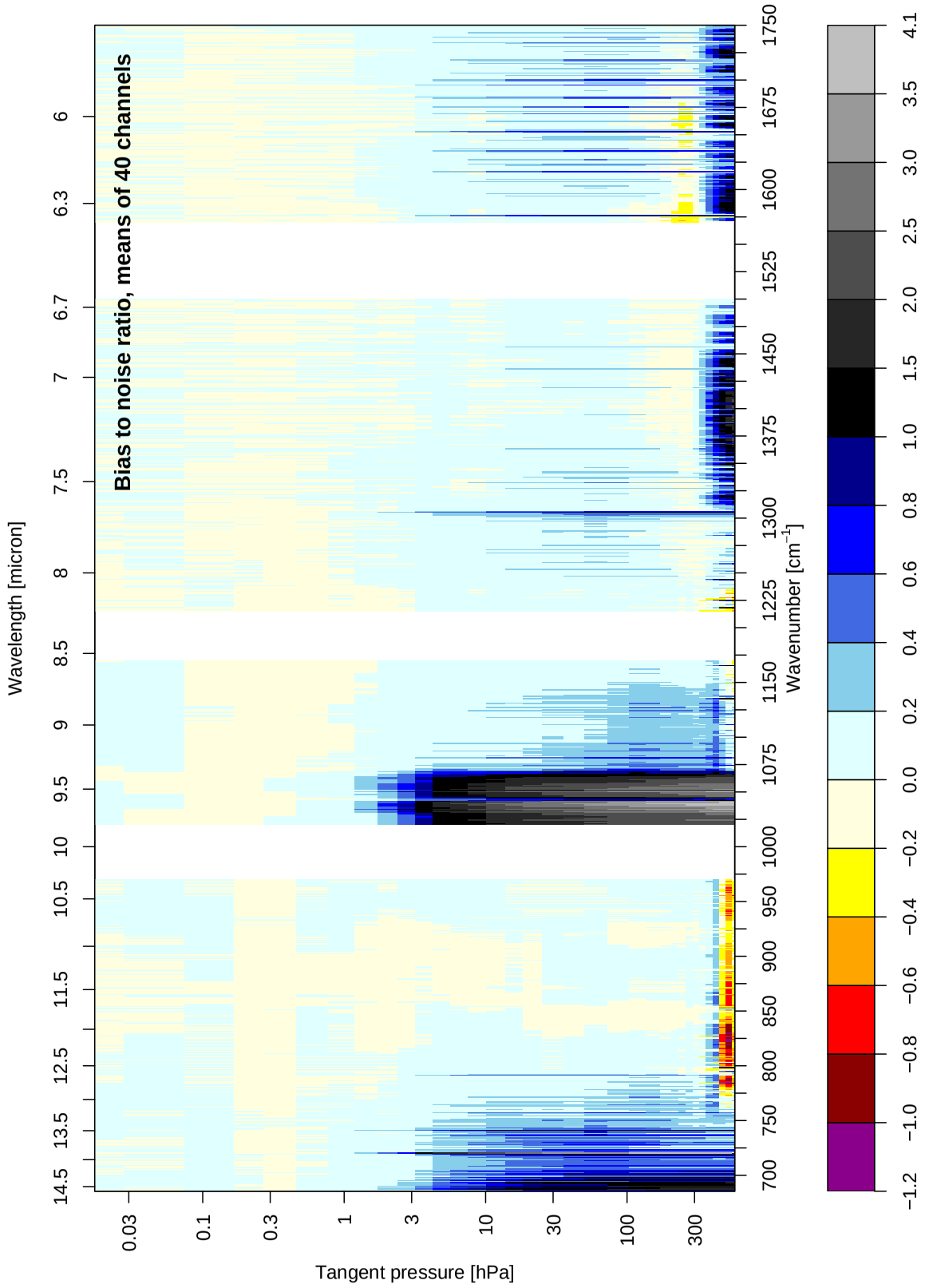

Figure 5: As Fig. 2, but for the mean bias to noise ratio (RTMIPAS-1d minus RFM-2d) over 40 channel intervals (i.e., 1 cm^{-1} intervals.

of the layer path lengths. To see this it is important to recall that the regression models for each RTMIPAS layer are based only on the LBL calculations for the 46 training profiles for all pencil beams with tangent points *below* that layer. This means much fewer cases are available for the lowest layers, and this by itself may lead to a poorer accuracy of the regression models. Consistent with this, the channels and tangent heights which show the poorest performance for RTMIPAS-2d are also the ones which showed the largest increases in the error-to-noise ratio when RTMIPAS-1d was evaluated for an independent profile set instead of the training profile set (BMH04). More importantly, the cases used to train the regression models for the lowest RTMIPAS-1d layers will not encounter the same variability in the layer path lengths as is present in RTMIPAS-2d. For example, in the extreme case of the lowest RTMIPAS layer, the variability in the layer path lengths in the horizontally homogeneous case arises only from the variability in refraction or the variability in layer depths, but the height of the layer boundaries and therefore the depth of the layer is horizontally constant for each atmospheric situation. In contrast, in the 2-dimensional case, the height of the RTMIPAS pressure levels and thus also the geometric depth of the layer may vary horizontally for each cross section. This means the layer path lengths can be much shorter or longer than is the case in horizontally homogeneous atmospheres, thus adding variability uncaptured in the training data. This problem does not occur for higher RTMIPAS layers, since cases from a larger range of pencil beams are available for the regression, and the variability in layer path lengths resulting from the range of tangent pressures is much larger than that from horizontally varying layer depths or sloping pressure levels. The poorer statistics for the lowest pencil beams suggest that it may be beneficial to retrain the regression models for the lowest RTMIPAS layers using LBL results for 2-dimensional atmospheres. However, many fields of view at these lower tangent altitudes are cloud contaminated and therefore will not be used in the assimilation, so such retraining is not considered a priority.

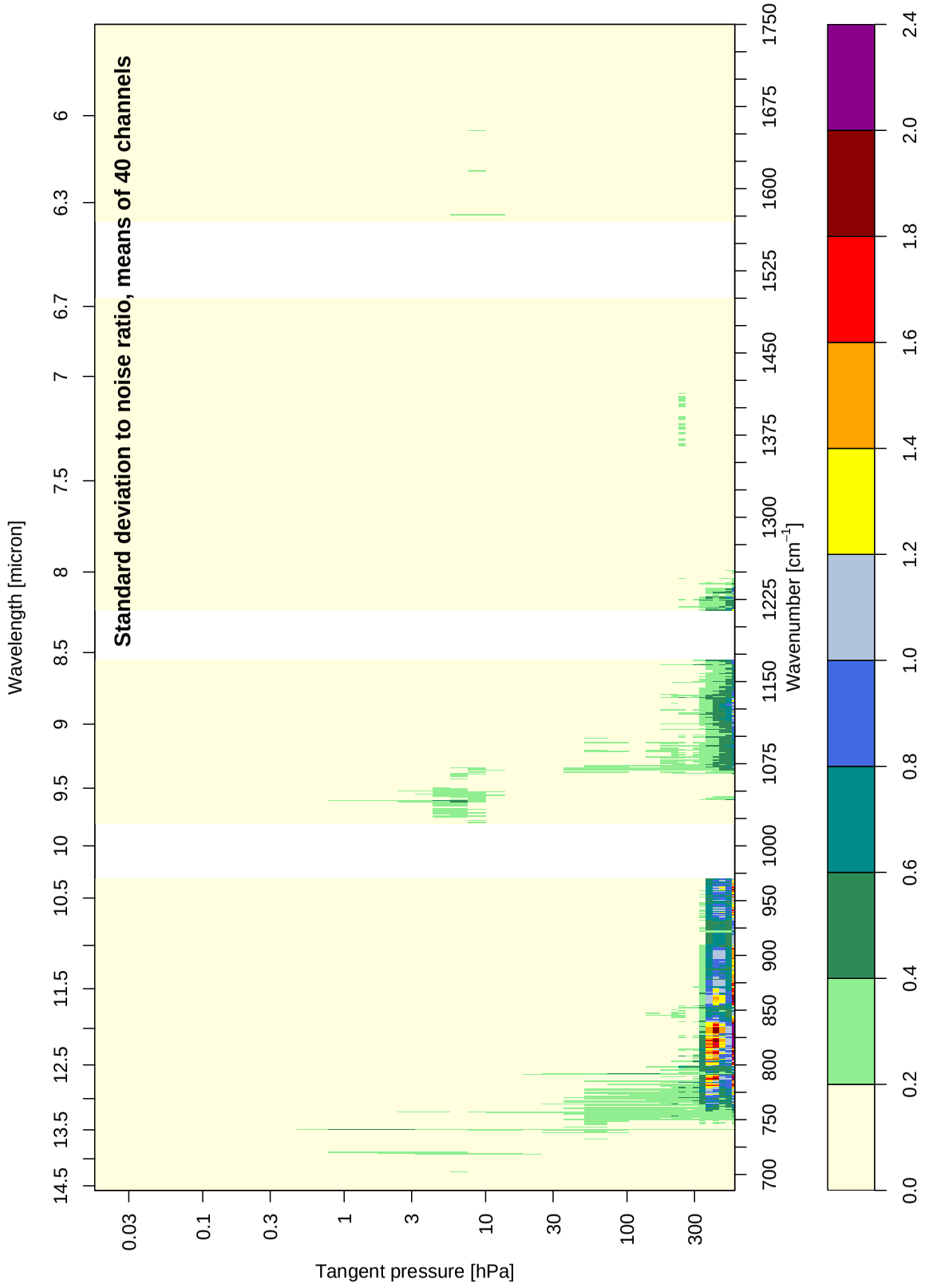

Figure 6: Standard deviation of the RTMIPAS-2d minus RFM radiance differences, scaled by the MIPAS noise, for the set of 40 diverse cross-sections. The plot shows the mean standard deviation to noise ratio over 40 channel intervals (i.e., 1 cm^{-1} intervals) as a function of wavenumber and pencil-beam pressure.

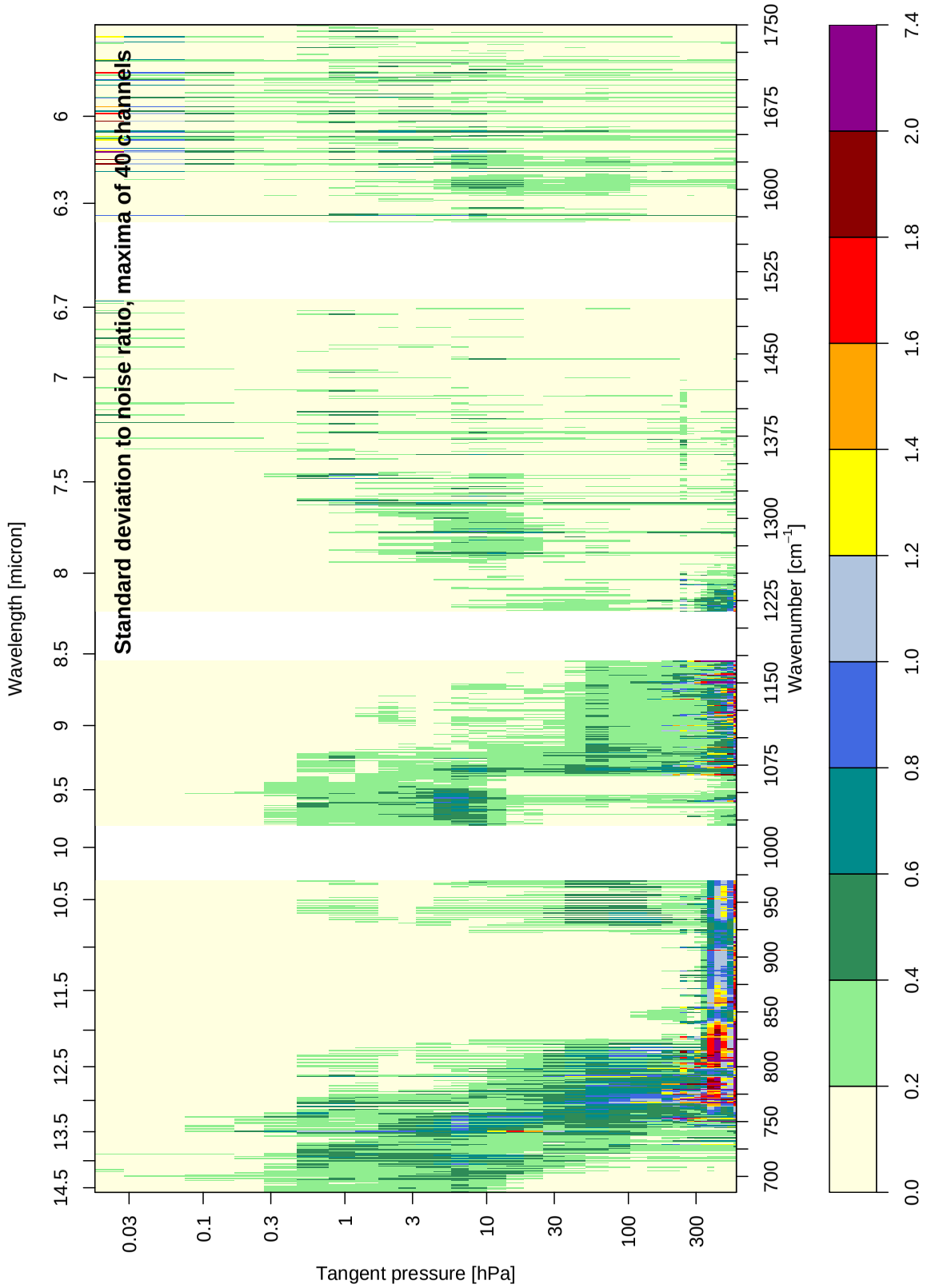

Figure 7: As Fig. 6, but for the maximum standard deviation to noise ratio over 40 channel intervals (i.e., 1 cm^{-1} intervals).

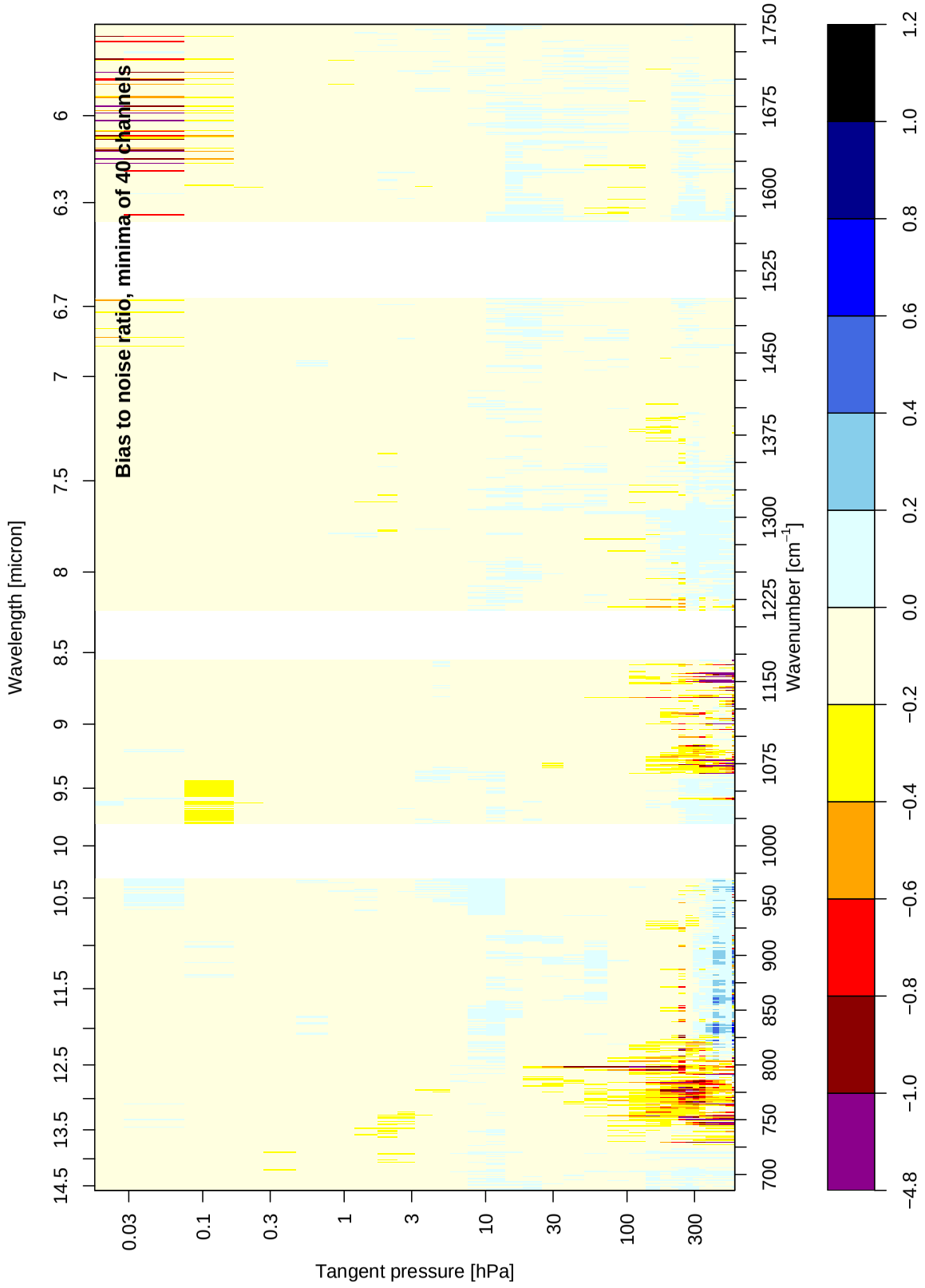

Figure 8: Mean RTMIPAS-2d minus RFM radiance differences (bias), scaled by the MIPAS noise, for the set of 40 diverse cross-sections. The plot shows the minimum of the bias to noise ratio of 40 channel intervals (i.e., 1 cm^{-1} intervals) as a function of wavenumber and pencil-beam pressure.

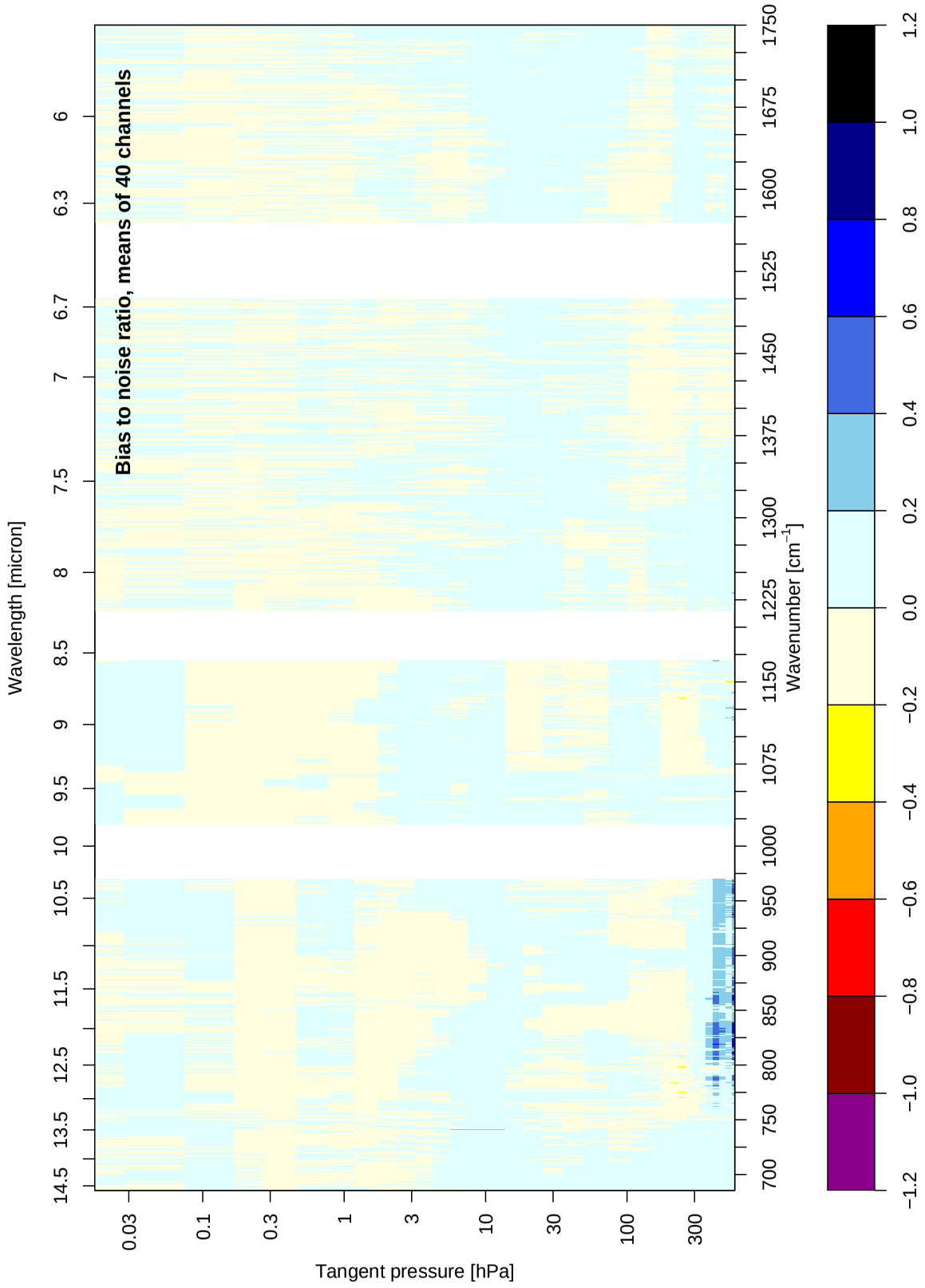

Figure 9: As Fig. 8, but for the mean bias to noise ratio over 40 channel intervals (i.e., 1 cm^{-1} intervals).

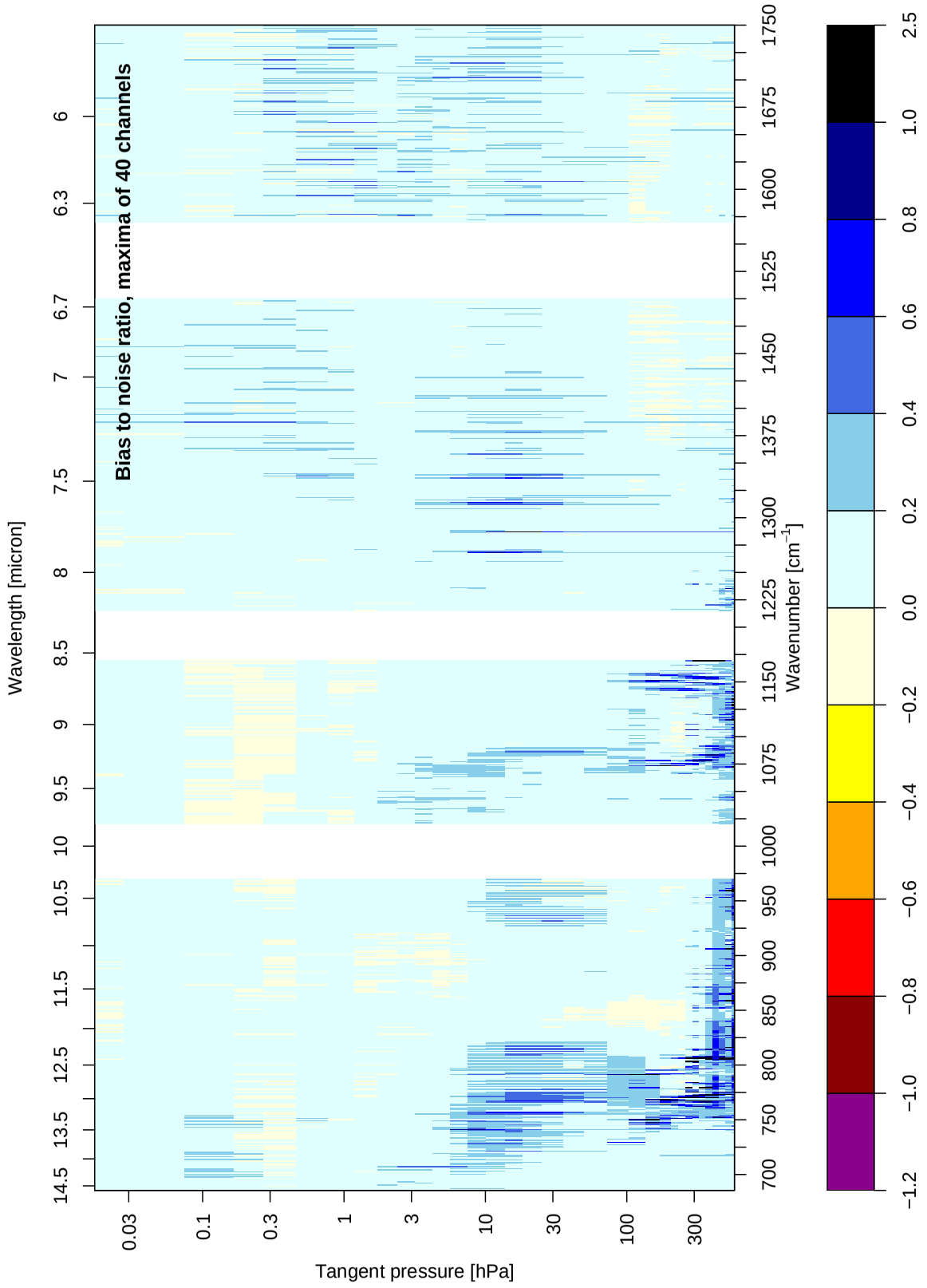

Figure 10: As Fig. 8, but for the maximum bias to noise ratio over 40 channel intervals (i.e., 1 cm^{-1} intervals).

3.3 Comparison of simulated and observed radiances

To further evaluate the benefits of RTMIPAS-2d we now present statistics from a comparison between observed MIPAS radiances and values simulated from ECMWF-model fields over two days. The comparisons are based on all available reprocessed MIPAS radiances (version 4.61) for the orbits 8216 to 8243 on 26 and 27 September 2003, resulting in a total of 1765 scans (orbits 8225, 8233, 8234, 8239 are missing). We consider only clear sweeps; cloudy sweeps are excluded based on the approach of Remedios and Spang (2002) and an additional threshold check on the clearest MIPAS channel (radiance in the 960.700 cm^{-1} channel below 125 $nW/(cm^2\ sr\ cm^{-1})$; Dudhia 2004, pers. communication). The atmospheric conditions for each scan were taken from ECMWF short-term forecasts, as would have been used as background data in the ECMWF assimilation system. The fields were interpolated to yield cross-sections for each MIPAS scan in the same way as for the 40 cross-sections described in section 2.4. The sub-tangent point of the central sweep in each scan was used to specify the location of the central profile, with the orientation of the cross-section given by the plane described by this sub-tangent point, the satellite's position, and the centre of the earth. For the RTMIPAS-1d calculations, only the central profile was used to specify the atmospheric conditions in a horizontally homogeneous manner. For the RTMIPAS-2d calculations, the full cross-section was used, and tangent point drift in the horizontal was taken into account. To locate the tangent point in the vertical, both calculations used the level-2 retrieved tangent pressures instead of the engineering pointing information. This is because considerable errors have been found in the engineering pointing information for MIPAS (von Clarmann et al. 2003).

We consider only a subset of MIPAS channels (Fig. 11), which is a set of channels expected to be used for assimilation studies. The channels have been selected using the method of Dudhia et al. (2002a) which iteratively grows microwindows[2] which maximise information content of the set of selected radiances relative to the error estimate in the *a priori* data. The method uses linear theory to estimate the retrieval error, given estimates for the error in the *a priori* data, the instrument noise, and error estimates from so-called systematic errors. The systematic errors include uncertainties or assumptions in the radiative transfer model, such as uncertainties in the spectroscopic data, neglecting the variability of certain gases, uncertainties in the instrument line shape, etc. We used the method to select 325 single-channel microwindows for a simultaneous retrieval of temperature, humidity, and ozone. The estimate for the ECMWF background error covariance matrix served to define the error in the *a priori* data, and in-flight values for the orbit 2081 were used to specify the MIPAS apodised instrument noise. Error sources considered for the systematic errors from unretrieved contributors were the same as in Dudhia et al. (2002a), except for the following differences: We included the error arising from the RTMIPAS fast transmittance calculation, and excluded the error arising from horizontal gradients. The error due to the climatological variability of the main 26 gases considered fixed in RTMIPAS is included, as well as errors arising from uncertainties in the tangent pressure specification (3 %). The reader is referred to Dudhia et al. (2002a) for more details. Note that in the following we present statistics for all tangent altitudes for each channel, regardless of the tangent altitude range selected by the microwindow selection.

Comparisons between observed and model-simulated radiances demonstrate the benefits of RTMIPAS-2d, achieved through a reduction in the forward model error in the radiative transfer calculations. For the lower tangent altitudes, standard deviations between model-simulated and observed MIPAS radiances are considerably smaller for the majority of the 325 channels when RTMIPAS-2d is used (Figure 12). At the same time, there is no significant increase in the standard deviation for any channel at any tangent altitude. Note that for the comparisons at the lowest tangent altitudes very few clear-sky sweeps are available so the statistics are less reliable. Biases between observed and model-simulated radiances are very similar for the RTMIPAS-2d and the RTMIPAS-1d calculations (not shown).

The reduction in the standard deviation is qualitatively consistent with theoretical estimates. Assuming the

[2] A microwindow is a set of radiances described by a spectral region and a tangent altitude range.

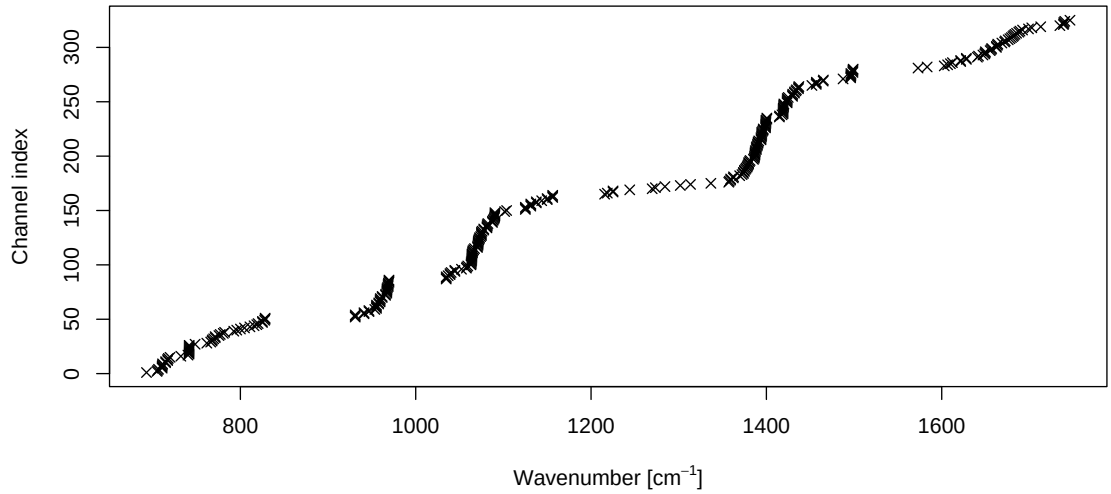

Figure 11: Wavenumbers [cm^{-1}] for the selected channels.

error introduced through the assumption of local horizontal homogeneity in RTMIPAS-1d is uncorrelated to other errors, we can estimate this error from the statistics shown in Figure 12 by taking the square root of the difference of the variances. This is shown in Fig. 13a, and can be compared to Fig. 13b which displays the noise-normalised standard deviations between RTMIPAS-1d and RFM-2d simulations for our 40 cross-sections used earlier. The two plots show good consistency, with similar spectral regions affected at similar tangent altitudes. For tangent altitudes above 20 km the estimate of the horizontal-gradient error from the observations appears somewhat smaller than that from the simulations. This is likely a result of different sampling (For instance, 10 of the 40 cross-sections were specifically sampled for considerable horizontal structure.). In contrast, for lower tangent altitudes (10 - 20 km), the observed horizontal-gradient error is larger than in the simulations in some spectral regions. This is likely the result of errors arising from the tangent point drift which is taken into account in the 2d-comparisons between model simulations and observations, but not in the simulations for the 40 cross-sections. Errors resulting from tangent-point drift are expected to be largest at lowest tangent altitudes.

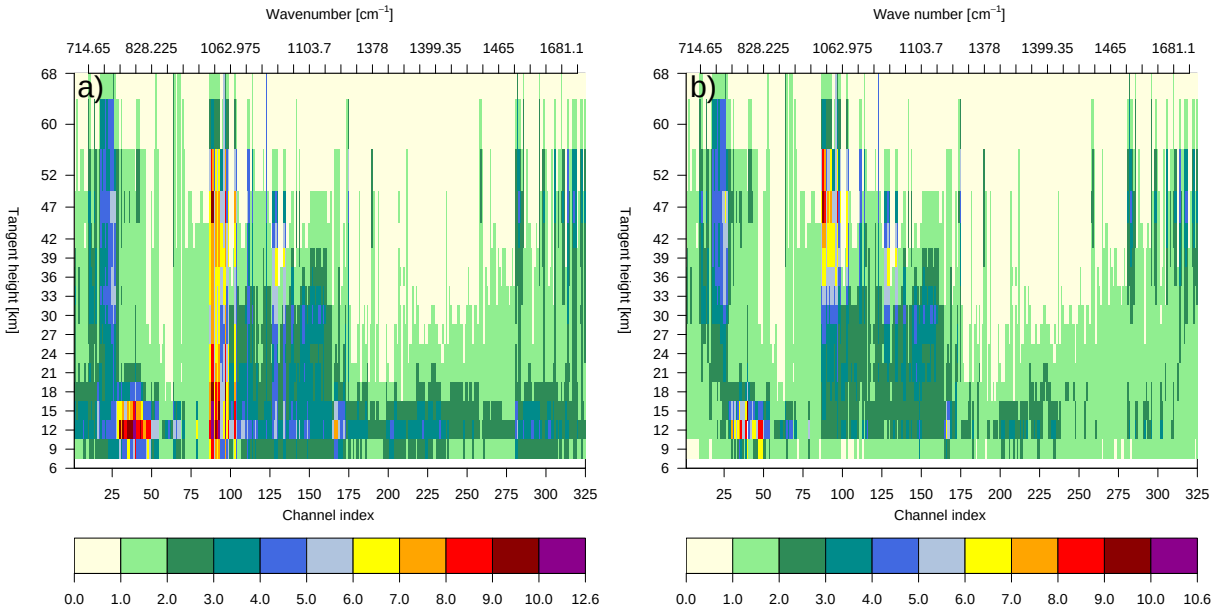

Figure 12: a) Noise-normalised standard deviation between simulated and observed clear MIPAS radiances for 26 and 27 September 2003 for the selected 325 channels. The simulated radiances are calculated assuming horizontal homogeneity. The lower x-axis gives the index of the channel used, whereas the upper x-axis gives examples of the wavenumbers for the channels shown. b) As a), but the simulated radiances were calculated from cross-sections, using RTMIPAS-2d.

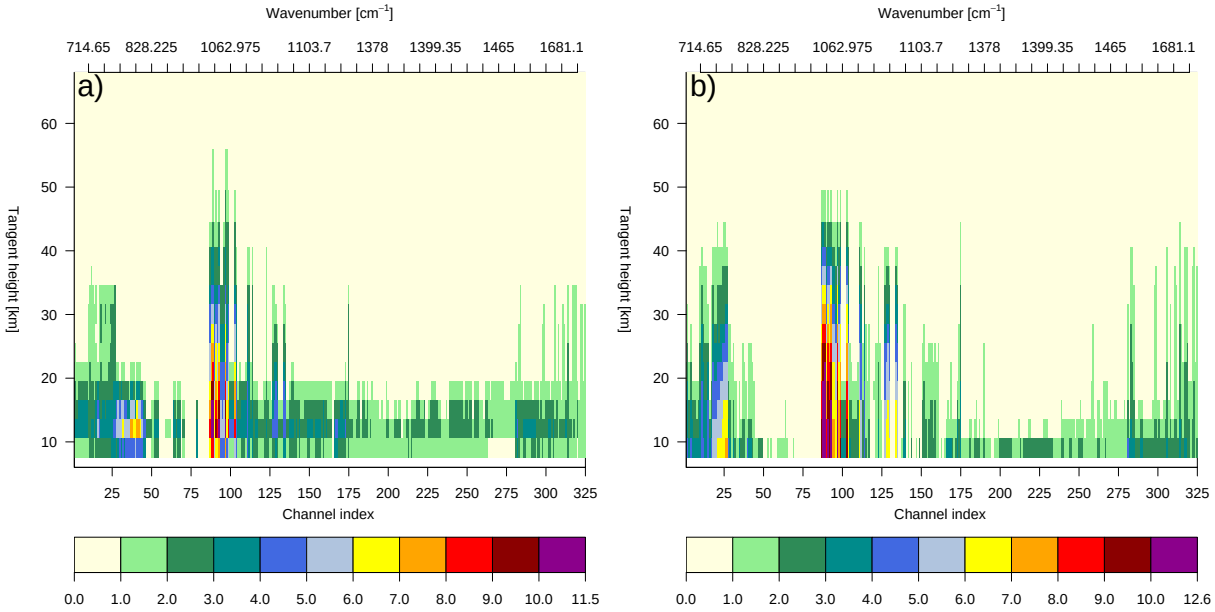

Figure 13: a) Noise-normalised error arising from assuming local horizontal homogeneity in the comparisons between observed and simulated FOV-convolved radiances shown in Fig. 12a and b. The lower x-axis gives the index of the channel used, whereas the upper x-axis gives examples of the wavenumbers for the channels shown. b) Noise-normalised error arising from assuming local horizontal homogeneity calculated from the comparison between RTMIPAS-1d and RFM-2d FOV-convolved radiances for 40 cross-sections for the selected 325 channels.

4 Summary and conclusions

In this report we have investigated the role of horizontal gradients in the atmosphere for the simulation of infrared limb radiances from the MIPAS instrument on-board the Envisat satellite, and investigated an extension of the RTMIPAS fast radiative transfer model designed to account for horizontal gradients. These aspects have been examined by comparing radiance spectra simulated with RTMIPAS to LBL equivalents and to real MIPAS observations. The main findings are:

- Neglecting horizontal gradients in the atmosphere can introduce errors in the radiance simulation that exceed by far the instrument noise. The problem is most severe for the lowest tangent heights, for which almost all channels exhibit errors due to horizontal gradients larger than the instrument noise.
- A pragmatic and cost-effective extension of the RTMIPAS fast forward model to the 2-dimensional geometry ('RTMIPAS-2d') can substantially reduce the error introduced if horizontal gradients are neglected. For tangent pressures less than 350 hPa almost all error due to horizontal gradients is eliminated, and RTMIPAS-2d is capable of simulating radiance spectra for 2-dimensional atmosphere to an accuracy that is below the noise level of the MIPAS instrument. In the pragmatic extension of RTMIPAS we account for the 2-dimensional geometry in the ray-tracing step, but use the regression coefficients originally derived from a set of horizontally homogeneous atmospheres. A fast method to perform ray tracing on a pressure grid has been developed, and the additional computations add only marginally to the execution time compared to RTMIPAS-1d.
- Radiances simulated with RTMIPAS-2d from cross-sections taken from ECMWF model fields show considerably smaller departures against observed MIPAS radiances than radiances simulated with RTMIPAS under the assumption of local horizontal homogeneity. The reduction is consistent with estimates from theoretical simulations.

Our results demonstrate that for tangent pressures less than 350 hPa (i.e., tangent altitudes below about 8 km) little could be gained by re-deriving the RTMIPAS regression coefficients based on LBL calculations for 2-dimensional atmospheres. In contrast, for tangent pressures larger than 350 hPa, retraining of the regression coefficients using 2-dimensional atmospheres may be beneficial in order to capture the additional variability, for instance, in the layer path lengths which are affected through horizontally varying layer depths. However, even without retraining the regression coefficients, RTMIPAS-2d provides a significant improvement for the radiance simulation compared to RTMIPAS-1d even for these lower pencil beams. Also, in practice the majority of the observations at tangent altitudes below 8 km are affected by clouds, and they will therefore not be used in the assimilation. A re-derivation of the coefficients based on LBL calculations for 2-dimensional atmospheres is thus not considered a priority.

The findings show that a significant reduction in the forward model error can be expected from using RTMIPAS-2d compared to RTMIPAS-1d in the planned assimilation of MIPAS limb radiances. Neglecting horizontal gradients introduces a considerable, and - by its nature - highly spectrally and possibly spatially correlated error in the radiance computations. At the same time, it has to be noted that not all channels will be used at lower tangent heights, and the error arising from horizontal gradients can be reduced at the data selection stage by excluding severely affected channels at certain tangent heights. This can be achieved in an objective way through data selection methods such as described by Dudhia et al. (2002a). Such data selection is necessary in any case since MIPAS provides a prohibitive number of channels for quantitative analyses. However, excluding observations strongly affected by horizontal gradients in the atmosphere also reduces information on these gradients that could otherwise be retrieved or assimilated from the observations.

Future work will investigate aspects of horizontal gradients further in the context of the direct assimilation of infrared limb radiances. While the reduction of forward model error is likely to be beneficial in the radiance assimilation, it is unclear to what extent information on atmospheric gradients in the radiances will improve the description of atmospheric gradients in the analysis, given the structure of the background error. In order to use RTMIPAS-2d in a variational data assimilation system, tangent linear and adjoint routines have been developed as for RTMIPAS-1d. We will report in the future in more detail on the horizontal aspects of limb radiance assimilation.

Acknowledgements

Niels Bormann was funded through the ASSET project (Assimilation of Envisat Data), a shared-cost project co-funded by the Research Directorate General of the European Commission within the activities of the Environment and Sustainable Development sub-programme of the 5th Framework Programme. Sean Healy is supported through the EUMETSAT/ECMWF Fellowship agreement. We are grateful to Anu Dudhia (Oxford University) for making the RFM available and for providing valuable support throughout this project. Richard Siddans (RAL) provided software to calculate the orientation of the MIPAS viewing planes. All MIPAS data used © ESA.

Appendix: Ray-tracing

The ray-tracing approach employed in RTMIPAS-2d can be viewed as a generalisation of the method outlined in BMH05 (Appendix A). From elementary geometry, if (r,θ) are the polar coordinates of a point P on the ray-path within a two-dimensional plane, the derivative of the distance along the ray-path, s, with respect to θ is

$$\frac{\mathrm{d}s}{\mathrm{d}\theta} = \frac{r}{\sin\phi} \tag{2}$$

where ϕ is angle between the local radius vector and the tangent to the ray-path at P (See Fig.3.5, Born and Wolf 1993).

Consider a point on ray-path, $P(i)$ that intersects the ith pressure level at the coordinate $r(i)$ and $\theta(i)$ and define the impact parameter at $P(i)$ as $a(i) = n(i)r(i)\sin\phi(i)$, where $n(i)$ is the refractive index. The total path between the ith and $(i+1)th$ pressure levels, Δs, is evaluated as the sum of the path-lengths along M sub-intervals (or integration steps) $\Delta s = \sum_{m=1}^{M} \delta s_m$ (Currently, $M = 10$). From eq.2 the path length along the mth sub-interval can be written as

$$\delta s_m \simeq l\,\delta\theta_m. \tag{3}$$

l is assumed to be a constant between the ith and $(i+1)th$ pressure levels, and is given by

$$l = \left(\frac{r(i) + r^*(i+1)}{\sin\phi(i) + \sin\phi^*(i+1)}\right) \tag{4}$$

where $r^*(i+1)$ is the radius of the $(i+1)th$ pressure level evaluated at $\theta(i)$; $\sin\phi(i) = a(i)/(n(i)r(i))$ and we approximate $\sin\phi^*(i+1) = a(i)/(n^*(i+1)r^*(i+1))$, noting that $n^*(i+1)$ is the refractive index on the $(i+1)th$ level, evaluated at $\theta(i)$.

The path between the ith and $(i+1)th$ pressure levels, which is composed of M steps, is characterised by angular positions (θ_m), impact parameter values (a_m) and ray-vector/radius vector angles (ϕ_m). When $m = 1$,

these variables are intialised with the values on the *ith* pressure level (e.g., $a_1 = a(i)$). As in the 1D-case, the change in angular position for the *mth* step can be written as,

$$\delta\theta_m = |\delta\phi_m| + |\delta\alpha_m| \tag{5}$$

where $\delta\alpha_m$ is the bending of the ray path caused by the gradients in the refractive index. However, in the 2D calculation the model variables on the fixed pressure levels (refractive index (n), refractivity (N), radius (r) and refractive index-radius product ($x = nr$)) have to be interpolated to θ_m, the angular coordinate of the starting point of the *mth* step, in order to evaluate $\delta\phi_m$ and $\delta\alpha_m$. We define

$$x_l = x_{i,\theta_m} + \frac{(m-1)}{M} \times (x_{i+1,\theta_m} - x_{i,\theta_m}) \tag{6}$$

and

$$x_u = x_{i,\theta_m} + \frac{m}{M} \times (x_{i+1,\theta_m} - x_{i,\theta_m}) \tag{7}$$

where x_{i,θ_m} and x_{i+1,θ_m} are the refractive index–radius product on the ith and $(i+1)th$ pressure levels, respectively, interpolated to θ_m. $\delta\phi_m$ is given by

$$\delta\phi_m = \phi_m - \phi_{m-1} \tag{8}$$

where $\phi_m = \sin^{-1}(a_m/x_u)$.

The ray bending, $\delta\alpha_m$, can be written as (e.g., eq. 9.41, Rodgers 2000)

$$\delta\alpha = -a_m \int_{x_l}^{x_u} \frac{\frac{d\ln n}{dx}}{\sqrt{(x^2 - a_m^2)}} dx \tag{9}$$

As in RTMIPAS-1d, this expression can be simplified by approximating $\sqrt{x^2 - a_m^2} \simeq \sqrt{2a_m(x - a_m)}$ and $\ln n \simeq 10^{-6}N$, where N is the refractivity, and it assumed that the variation of N at θ_m, between x_l and x_u, has the form $N(x) = N_m \exp(-k_m(x - x_l))$. Eq.9 then becomes

$$\delta\alpha = 10^{-6} k_m N_m \exp(k_m(x - a_m)) \sqrt{\frac{a_m}{2}} \int_{x_l}^{x_u} \frac{\exp(-k_m(x - a_m))}{\sqrt{(x - a_m)}} \mathrm{d}x. \tag{10}$$

This has an analytical solution

$$\delta\alpha = 10^{-6} \sqrt{\frac{\pi a_m k_m}{2}} N_m \exp(k_m(x_l - a_m)) \left[\mathrm{erf}(\sqrt{k_m(x_u - a_m)}) - \mathrm{erf}(\sqrt{k_m(x_l - a_m)}) \right] \tag{11}$$

where "erf" denotes the Gaussian error function. The angular coordinate is updated for the $(m+1)th$ step using $\theta_{m+1} \rightarrow \theta_m + \delta\theta_m$ and the impact parameter a is updated with

$$a_{m+1} = a_m + \left(\frac{\partial n}{\partial \theta} \right)_r \delta s_m \tag{12}$$

References

Bormann, N., M. Matricardi, and S. B. Healy, 2004: RTMIPAS: A fast radiative transfer model for the assimilation of infrared limb radiances from MIPAS. Technical Memorandum 436, ECMWF, Reading, UK, 49 pp [available under www.ecmwf.int/publications/library/do/references/list/14].

Bormann, N., M. Matricardi, and S. B. Healy, 2005: A fast radiative transfer model for the assimilation of infrared limb radiances from MIPAS. *Quart. J. Roy. Meteor. Soc.*, **131**, in press.

Born, M., and E. Wolf, 1993: *Principles of Optics*. Pergamon Press, Oxford, U.K., 836 pp.

Carlotti, M., B. Dinelli, P. Raspollini, and M. Ridolfi, 2001: Geo-fit approach to the analysis of limb-scanning satellite measurements. *Applied Optics*, **40**, 1872–1885.

Chevallier, F., 2002: Sampled database of 60-level atmospheric profiles from the ECMWF analyses. NWP SAF Report 4, ECMWF, Reading, U.K., 27 pp [available under www.ecmwf.int/publications/library/do/references/list/202].

Dethof, A., 2003: Assimilation of ozone retrievals from the MIPAS instrument on board ENVISAT. Technical Memorandum 428, ECMWF, Reading, UK, 19 pp [available under www.ecmwf.int/publications/library/do/references/list/14].

Dudhia, A., V. L. Jay, and C. D. Rodgers, 2002: Microwindow selection for high-spectral-resolution sounders. *Applied Optics*, **41**, 3665–3673.

Dudhia, A., P. Morris, and R. Wells, 2002: Fast monochromatic radiative transfer calculations for limb sounding. *J. Quant. Spectrosc. Radiat. Transfer*, **74**, 745–756.

ESA, 2000: ENVISAT-MIPAS: An instrument for atmospheric chemistry and climate research. ESA report SP-1229, European Space Research and Technology Centre, Noordwijk, The Netherlands, 124 pp.

Gille, J., and F. House, 1971: On the inversion of limb radiance measurements I: Temperature and thickness. *J. Atmos. Sci.*, **28**, 1427–1442.

Healy, S., 2001: Radio occultation bending angle and impact parameter errors caused by horizontal refractive index gradients in the troposphere: A simulation study. *J. Geophys. Res.*, **106**, 11875–11889.

Kidder, S. Q., and T. H. Vonder Haar, 1995: *Satellite Meteorology: An introduction*. Academic press, London, UK, 466 pp.

Livesey, N., and W. Read, 2000: Direct retrieval of line-of-sight atmospheric structure from limb sounding observations. *Geophys. Res. Lett.*, **27**, 891–894.

Livesey, N., and D. Wu, 1999: EOS MLS retrieval process algorithm theoretical basis. Technical Report (ATBD-MLS-03) JPL D-16159, Jet Propulsion Laboratory, California Institute of Technology, Pasadena, California 91109-8099, USA, 84 pp.

Marks, C. J., and C. D. Rodgers, 1993: A retrieval method for atmospheric composition from limb emission measurements. *J. Geophys. Res.*, **98 D8**, 14,939–14,953.

Matricardi, M., F. Chevallier, and J.-N. Thépaut, 2004: An improved general fast radiative transfer model for the assimilation of radiance observations. *Quart. J. Roy. Meteor. Soc.*, **130**, 153–173.

Reburn, W., V. Jay, R. Siddans, and B. Kerridge, 2003: Tomographic limb-sounding of the upper troposphere and lower stratosphere. In Abstracts of the 2003 EGS - AGU - EUG Joint Assembly, Nice France, EGS/AGU/EGU, abstract no. 11561.

Remedios, J., and R. Spang, 2002: MIPAS observations of clouds and their effects on level 2 trace gas products. In Envisat Validation Workshop, Frascati, Italy, ESA, [available online under envisat.esa.int/pub/ESA_DOC/envisat_val_1202/proceedings/ACV/MIPAS/05_remedios.pdf].

Ridolfi, M., B. Carli, M. Carlotti, T. von Clarmann, B. Dinelli, A. Dudhia, J.-M. Flaud, M. Höpfner, P. Morris, P. Raspollini, G. Stiller, and R. Wells, 2000: Optimized forward model and retrieval scheme for MIPAS near-real-time data processing. *Applied Optics*, **39**, 1323–1340.

Ridolfi, M., L. Magnani, M. Carlotti, and B. Dinelli, 2004: MIPAS-ENISAT limb-sounding measurements: Trade-off study for improvement of horizontal resolution. *Applied Optics*, **43**, 5814–5824.

Rodgers, C. D., 2000: *Inverse methods for atmospheric sounding: Theory and practice*. World Scientific Publishing, Singapore, New Jersey, London, Hong Kong, 256 pp.

Saunders, R., M. Matricardi, and P. Brunel, 1999: An improved fast radiative transfer model for assimilation of satellite radiance observations. *Quart. J. Roy. Meteor. Soc.*, **125**, 1407–1426.

von Clarmann, T., S. Ceccherini, A. Doicu, A. Dudhia, B. Funke, U. Grabowski, S.Hilders, V. Jay, A. Linden, M. López-Puertas, F. Martin-Torres, V. Payne, J. Reburn, M. Ridolfi, F. Schreier, G. Schwarz, R. Siddans, and T. Steck, 2003: A blind test retrieval experiment for infrared limb emission spectrometry. *J. Geophys. Res.*, **108 D23**, doi:10.1029/2003JD003835.

von Clarmann, T., N. Glatthor, U. Grabowski, M. Höpfner, S. Kellmann, M. Kiefer, A. Linden, G. Tsidu, M. Milz, T. Steck, G. Stiller, D. Wang, H. Fischer, B. Funke, S. Gil-López, and M. López-Puertas, 2003: Retrieval of temperature and tangent alititude pointing from limb emission spectra recorded from space by the Michelson Interferometer for Passive Atmospheric Sounding (MIPAS). *J. Geophys. Res.*, **108 D23**, doi:10.1029/2003JD003602.